Theoretical and Experimental Predictions of First-Ply Failure of a Laminated Composite Elevated Floor Plate

R R Chang and T H Chiang

Proceedings of the Institution of Mechanical Engineers, Part E: Journal of Process Mechanical Engineering 2010 224: 233
DOI: 10.1243/09544089JPME327

Theoretical and experimental predictions of first-ply failure of a laminated composite elevated floor plate

R R Chang[1]* and **T H Chiang**[2]
[1]Department of Mechanical Engineering, China University of Science Technology, Taipei, Republic of China
[2]Department of Mechanical Engineering, National Chiao Tung University, Hsin-Chu, Republic of China

The manuscript was received on 17 November 2009 and was accepted after revision for publication on 12 April 2010.

DOI: 10.1243/09544089JPME327

Abstract: Experimental and theoretical approaches are studied via the first-ply failure strength on anti-symmetrically laminated composite elevated floor plates with various length-to-depth ratios, aspect ratios, and optimal fibre orientations subjected to central point loads. Optimal angle-ply orientations of anti-symmetric $[\theta/-\theta\ldots]_{-S}$ laminated composite plates designed for maximum stiffness were investigated. A vacuum-assisted resin transfer moulding (VARTM) technique was used to manufacture an elevated floor plate by the stacking of pieces of glass-fibre fabrics in a vacuum pressure mould. In VARTM, resin is injected under pressure into a rigid mould filled with fibre preform and subsequent curing. The failure modes of the composite plates were studied, and the experimental results were used to verify the theoretical predictions. The first-ply failure loads of the composite plates are determined using the acoustic emission AMS3 system. The results have been proved to be efficient and effective in the theoretical and experimental analyses of first-ply failure loads of the composite plates.

Keywords: laminated composite elevated floor plate, optimal angle ply, first-ply failure, vacuum-assisted resin transfer moulding, maximum stiffness, fibre perform

1 INTRODUCTION

Elevated floors have been gaining widespread usage and prominence in view of the wide computer equipment and are used in buildings. These elevated floors are designed to be supported on pedestals at the corners of elevated floors so as to present an access space between the elevated floor and the building supporting structure that can be used to run electrical cabling, computer lines, air conditioning, or other heating systems. Among these elevated floors, a common feature is that they must undergo certain heavy static and rolling loads with an appropriate safety factor and low maintenance costs. In the past, many products have been made in reducing the weight of elevated floors by using more advanced aluminium alloys, more optimized designs, and more sophisticated manufacturing methods [**1**–**5**]. However, aluminium designs are limited in their ultimate stiffness/strength-to-weight ratios by the inherent mechanical properties of aluminium. On the contrary, composite material has the merits of excellent strength-to-weight ratio and controlled anisotropy property which overcomes the general disadvantages caused by the conventional type of metal elevated floors.

For reliability assurance, prediction of the failure process of laminated composite structures and the maximum loads that the structures can withstand before failure occurs has thus become an important research topic. Ikegami *et al.* [**6**] developed the failure criterion of angle-ply laminates that was derived from the experimental results of filament-wound tubes made from a glass-fibre/epoxy resin composite. The most popular failure criteria, as discussed by Soni [**7**], are the maximum stress criterion, maximum strain criterion, and quadratic polynomial criteria such as the Tsai–Wu, Hoffman, and Hill criteria. Reddy and his associates [**8**, **9**] used the finite-element method to calculate the linear and non-linear first-ply failure loads of laminated composite plates according to several phenomenological failure criteria. Most of their works, however, have been limited to theoretical

*Corresponding author: Department of Mechanical Engineering, China University of Science Technology, No. 245 Sec. 3, Yen-Chu Yuan Road, Taipei, Republic of China.
email: chang@cc.cust.edu.tw

investigation, and results so obtained have not been verified by experiment. For safety reasons, composite elevated floor plates must be designed and manufactured for high reliability. A meaningful reliability assessment of a composite elevated floor plate relies on the accuracy of the theoretical and practical predictions of the first-ply failure strength. Therefore, in search of a proper failure criterion, the capabilities of the failure criteria in predicting reliable first-ply failure load of a composite plate are investigated in this article. Several studies have investigated the first-ply failure strength of laminated composite parts by using an acoustic emission (AE) system (AMS3). For instance, Kam *et al.* [**10–12**] studied the linear and non-linear first-ply failure strengths of cross-ply laminated composite plates using both theoretical and experimental approaches. Chang and Chu [**13**, **14**] have recently developed the first-ply failure loads of laminated composite pressure vessels and laminated composite shafts, which are determined using an AE system.

In order to utilize the composite material, the composite structure must be optimized with proper fibre orientation. In this article, the ANSYS finite-element program [**15**] is extended to the study of optimal angle-ply orientations and depth of the base rib of a composite plate with maximum stiffness subjected to central load. A C^0 finite element for a laminated composite plate, which is derived from the first-order shear deformation theory [**16**], is used in the plate frame. The effects of various length-to-depth ratios and aspect ratios upon the optimal lamination arrangements are investigated by means of a number of examples. In this work, a three-dimensional (3D) elevated floor plate is manufactured with glass-fibre-reinforced epoxy composite materials by the vacuum-assisted resin transfer moulding (VARTM) process. First-ply failure load and deformation of a composite plate are also studied via both experimental and analytical approaches. Experimental investigation of first-ply failure strength of a composite plate subjected to static transverse central loads is performed and monitored by an AE technique. A comparison between the experimental approaches and the analytical methods is made to demonstrate the suitability of the proper failure criteria in predicting first-ply failure strength.

2 COMPOSITE ELEVATED FLOOR PLATE

The plate body is treated as a rectangular composite elevated floor plate that has a continuous flat top surface panel of area $a \times b$ and constant thickness h (Fig. 1). The continuous plate is provided with a smooth rectangular surface panel and peripheral border flange or base rib of depth L projecting downwards around the periphery of the panel, and space slightly inwards from the edges of the panel. A schematic description of the finite-element mesh and applied loading of the composite plate are shown in Fig. 1(a). The finite-element method formulated on the basis of first-order shear deformation theory [**16**] is used to evaluate the stress distribution in the composite plate. In the finite-element analysis of the composite plate, 180 rectangular plate elements and 581×5 degrees of freedom were used to model the composite plate. In this study, an eight-node rectangular isoparametric element with reduced integration 1×1 Gauss rule is used to integrate the shear stiffness terms, whereas that with 2×2 Gauss rule is used to integrate the bending and inertia stiffness terms; it contains five degrees of freedom (three displacements and two slopes, i.e. shear rotations) per node. The reference (X, Y, Z) and material (1, 2, 3) co-ordinate systems lie in the mid-plane of the plate being normal to the mid-plane, as shown in Fig. 1(b). It is noted that the slope of the surface is discontinuous at the interface between any two neighbouring segments with different cross-sections. For the eight-node element there are four Gauss points. Figure 1(c) shows the scheme used to number the Gauss points for an eight-node element. The boundary conditions of the composite plate are shown in Fig. 1(d). The stress resultants in the geometric co-ordinates are given in reference [**17**]

$$\begin{aligned} N_i &= A_{ij}\varepsilon_j + B_{ij}k_j \\ M_i &= B_{ij}\varepsilon_j + D_{ij}k_j \\ Q_i &= \overline{Aij}\varepsilon_j \end{aligned} \tag{1}$$

where N_i denotes the in-plane stress results, M_i represents the moment results, and Q_i denotes the transverse shear stress results. A_{ij}, B_{ij}, D_{ij} $(i, j = 1, 2, 6)$, and $\overline{Aij}$ $(i, j = 4, 5)$ are the in-plane stiffness, bending in-plane coupling stiffness, twist coupling stiffness, and thickness-shear stiffness, respectively. The material components are given by

$$(A_{ij}, B_{ij}, D_{ij}) = \sum_{m=1}^{\mathrm{NL}} \int_{Z_m}^{Z_{m+1}} Q_{ij}^{(m)}(1, Z, Z^2)\mathrm{d}Z \qquad (i, j = 1, 2, 6) \tag{2}$$

$$\overline{A_{ij}} = \sum_{m=1}^{\mathrm{NL}} \int_{Z_m}^{Z_{m+1}} k_\alpha k_\beta Q_{ij}^{(m)}\mathrm{d}Z \qquad (i, j = 4, 5; \alpha = 6 - i; \beta = 6 - j) \tag{3}$$

Here, Z_m denotes the distance from the mid-plane to the lower surface of the mth layer and NL is the total number of layers. The stiffness coefficients $Q_{ij}^{(m)}$ vary with the material properties and orientation of the mth layer group, and the parameters k_α and k_β are shear correction factors. For homogenous plates $k_1 = k_2 = 5/6$, the classic value was determined by Reissner [**18**].

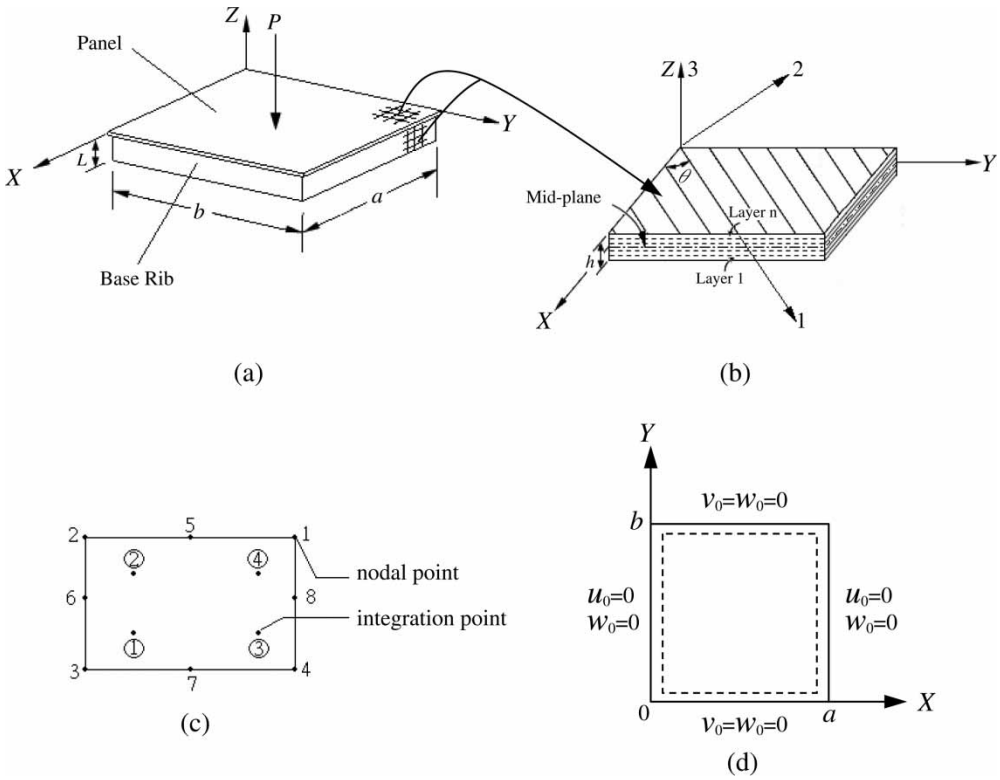

Fig. 1 Schematic description of the finite element for the composite elevated floor plate: (a) finite element mesh, (b) definition of reference (X, Y, Z) and material $(1, 2, 3)$ co-ordinate systems, (c) eight-node element, and (d) boundary conditions of a simply supported plate

3 FIRST-PLY FAILURE ANALYSIS OF COMPOSITE PLATES

The failure criteria for composite materials can be classified into two groups: independent failure criteria and polynomial failure criteria. The maximum strain and maximum stress criteria are the independent failure criteria, while the Hoffman, Hill, and Tsai–Wu failure criteria are the tensor polynomial failure criteria. Herein, a number of phenomenological failure criteria [**8**, **9**] are adopted in the analysis. The first-ply failure analysis of the laminated composite plate is performed via the use of a suitable failure criterion. Determination of first-ply failure loads of laminated composite plates is made using the maximum stress, maximum strain, Hoffman, Tsai–Hill, and Tsai–Wu failure criteria. The first-ply failure analysis is performed under the assumption that a given ply would fail if the failure index at any point within the ply reaches a value of unity. Therefore, the first-ply failure can be calculated according to four different failure criteria which are reported in reference [**8**]. It should be noted that these criteria are presented in 3D stress space. All the components are referred to the material co-ordinates.

4 PROBLEM FORMULATION

The objective in the present optimal design of a laminated composite plate with a given thickness h and number of layer groups NL is the selection of the fibre angle and the depth of the base rib that gives the maximum stiffness of the plate. The ANSYS linear finite-element program was employed in the numerical analysis of the simply supported plate comprising layers of equal thickness ($h_i = h/\mathrm{NL}$) subject to a centre point load. The material properties and the dimensions of the simply supported plate used in the following optimum design are given in Table 1. It is assumed that $G_{13} = G_{12}$, $\nu_{12} = \nu_{13}$, fibre volume $V_\mathrm{f} = 0.64$, and density $\rho = 1.0$ in which 1, 2, and 3 directions are principal material property directions, as shown in Fig. 1(b). Optimal angle-ply orientations of composite plates designed for maximum stiffness subjected to centre point load were investigated. In the linear finite-element analysis, a model of 180 rectangular plate elements was used. The relationships between deflections and lamination angles of anti-symmetric fibre lay-ups $[\theta/-\theta/\theta]_{-3\mathrm{S}}$ with various geometry and loading conditions were studied. The optimization criterion used here is that of minimum deflection, which is equivalent to the criterion of maximum stiffness. In

Table 1 Material properties and plate dimensions used for optimum design

Material constants		Strengths	
E_1 (GPa)	26.302	X_T (MPa)	324.179
E_2 (GPa)	26.302	X_C (MPa)	107.818
E_3 (GPa)	26.302	$Y_T = Z_T$ (MPa)	324.179
$G_{12} = G_{13}$ (GPa)	3.062	$Y_C = Z_C$ (MPa)	107.818
G_{23} (GPa)	1.531	R (MPa)	34.761
$\nu_{12} = \nu_{13}$	0.124	$S = T$ (MPa)	44.569
Plate		*Values*	
Thickness, h (mm)		4.68	
Number of layers (NL)		18	
Ply thickness, $h_i = h/NL$ (mm)		0.26	

mathematical form, the optimization problem

$$\begin{aligned} &\text{Minimize} \quad \Phi(\boldsymbol{\theta}, L) = W/W^0 \\ &\text{Subject to} \quad 0^\circ \leqslant \theta_i \leqslant 180^\circ, \quad i = 1, \ldots, \text{NL} \\ &\qquad\qquad\quad 0 \leqslant L \end{aligned} \tag{4}$$

where Φ is a objective function, $\boldsymbol{\theta}$ is a vector of the fibre layer directions and $\boldsymbol{\theta} = (\theta_1, \theta_2, \ldots, \theta_{\text{NL}})^{\text{T}}$, L is the depth of the base rib, NL is the number of layers, W is the transverse deflection of the simply supported floor plate, and W^0 is the reference value of W. The above optimization problem can be solved by a multi-level approach in which the problem is transformed into a two-level problem and the design space $\{\boldsymbol{\theta}, L\}$ is replaced by two design spaces in $\boldsymbol{\theta}$ and L, respectively. At the first level, the objective function $\Phi(\boldsymbol{\theta}, L)$ in equation (4) is transformed into a single parameter objective function $\Phi_1(\boldsymbol{\theta})$ and the objective is to find the fibre layer directions that minimize the value of the objective function. The second-level problem is to minimize another single-parameter objective function $\Phi_2(L)$ by determining the depth of the base rib while the fibre layer directions obtained at the previous level of optimization are unaltered at this stage. A schematic description of the proposed multi-level approach is given in Fig. 2. Results are obtained by iterating between the two levels of optimization.

1. First-level problem: At the first level, the objective is to find the optimal angle-ply orientation of each fibre layer, which minimizes the transverse deflection of the plate for a given central load. The optimal fibre layer directions are determined by solving the

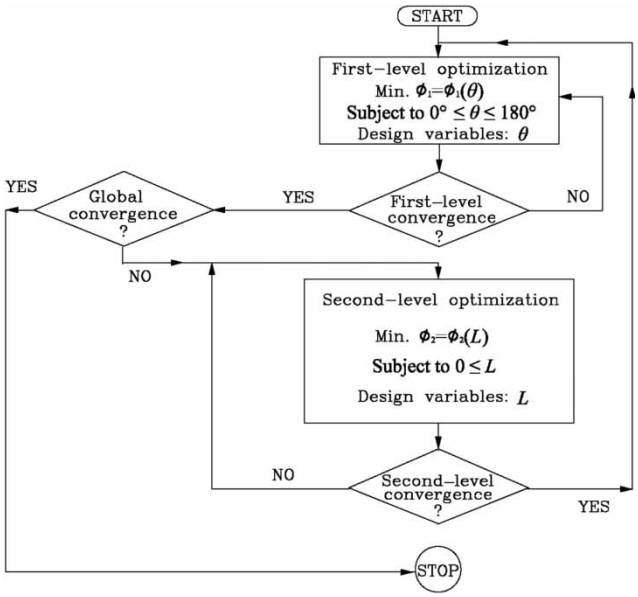

Fig. 2 Multi-level design procedure

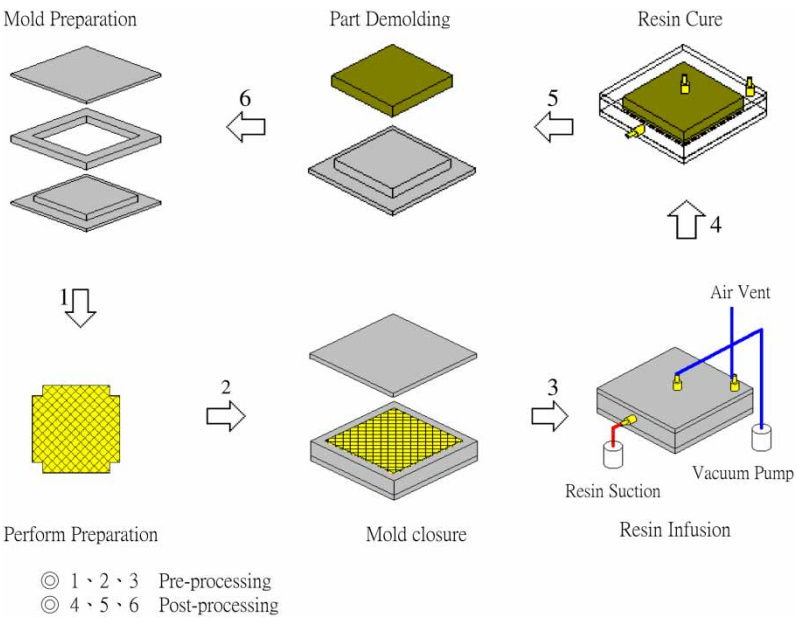

Fig. 3 Six stages of the VARTM process

following minimization problem

$$\begin{aligned} &\text{Minimize} \quad \Phi_1(\boldsymbol{\theta}) = W/W^0 \\ &\text{Subject to} \quad 0^\circ \leqslant \theta_i \leqslant 180^\circ, \quad i = 1, \ldots, \text{NL} \\ &\qquad\qquad L = \bar{L}, \quad 0 \leqslant \bar{L} \end{aligned} \tag{5}$$

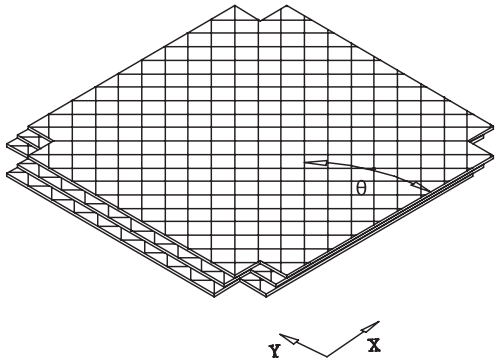

(a)

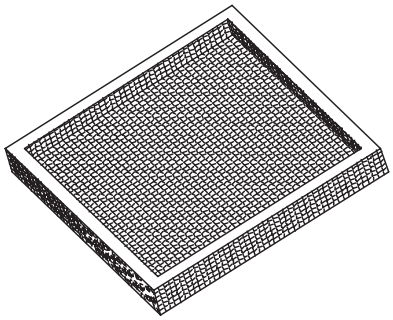

(b)

Fig. 4 Configurations of (a) the development drawing of the composite elevated floor plate and (b) its preform

During the minimization process, a 1D minimum search using a direct root method [**19**] is used to locate the new position of the design variables in the design space while the depth of the base rib $\bar{L}$ is obtained at the previous level of optimization. When the optimal solution at this level is obtained, the design process then goes to the second level of optimization that follows.

2. Second-level problem: At this level, the fibre layer directions obtained previously are kept constant and the objective is to determine the depth of the base rib so that the total deflection of the plate is minimized. The minimization problem is defined in the following mathematical form

$$\begin{aligned} &\text{Minimize} \quad \Phi_2(L) = W/W^0 \\ &\text{Subject to} \quad 0 \leqslant L \\ &\qquad\qquad \theta_i = \boldsymbol{\theta}_i, \quad i = 1, \ldots, \text{NL} \end{aligned} \tag{6}$$

This optimization procedure is similar to the first-level method; the previous level optimal solution $\boldsymbol{\theta}_i$ is used as the starting point and the direct root method is used to search the design variables to determine the true optimal solution of the problem.

5 EXPERIMENTAL INVESTIGATION

5.1 VARTM fabrication process

VARTM is an advanced composite processing technology for manufacturing high-quality composite structures. In the past, different types of composite structures have been designed and manufactured by RTM or VARTM [**20**–**25**]. In this work, a VARTM technique was used to manufacture an elevated floor plate by stacking pieces of glass-fibre fabrics or preform in

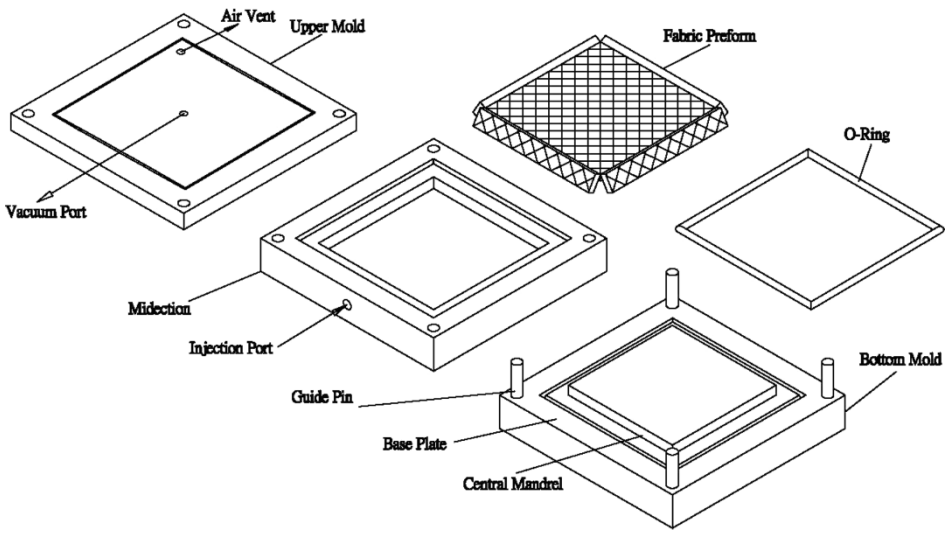

Fig. 5 Mould for manufacture of the composite elevated floor plate

a vacuum pressure mould. Then, the resin is injected into this preform under moderate pressure, often with the assistance of a vacuum pump to evacuate the mould, to enhance the flow. Figure 3 shows the important pre-processing and post-processing steps of the VARTM process. The plate system defines a smooth rectangular surface panel and a peripheral border flange or base rib projecting downwards around the periphery of the surface panel and spaced slightly inward from the edges of the surface panel. The composite plate is an anti-symmetric fibre lay-up $[\theta/-\theta\ldots]_{-S}$ structure that extends around the entire peripheral border flange or base rib.

The VARTM process involves the following six stages:

1. Cleaning the mould with acetone and spraying mould-release.
2. Cutting and pressing the dry glass-fibre weaves into desired shapes that when assembled generally conform to the surfaces of the finished structure (see Figs 4(a) and (b)). It should be noted that the optimal angle-ply angles θ with respect to the axis of the composite plate are used to design the maximum stiffness subjected to central load.
3. Filling up the mould with the preform. The mould includes a base, bottom mould, mid-section, upper mould, central mandrel, seal, guide pin, injection port, vacuum port, air port, and fabric preform assembled, as shown in Fig. 5.
4. Sealing off the mould and running vacuum. An air pressure of 0.5 MPa and a vacuum pressure of 1.0 torr were applied to the resin bath and the sealed mould, respectively.
5. Curing of the product. The curing pressure is about 0.5 MPa and the temperature is about 90–120 °C for about 90 min to 2 h. The curing of the resin was performed under the cure cycle, shown in Fig. 6.

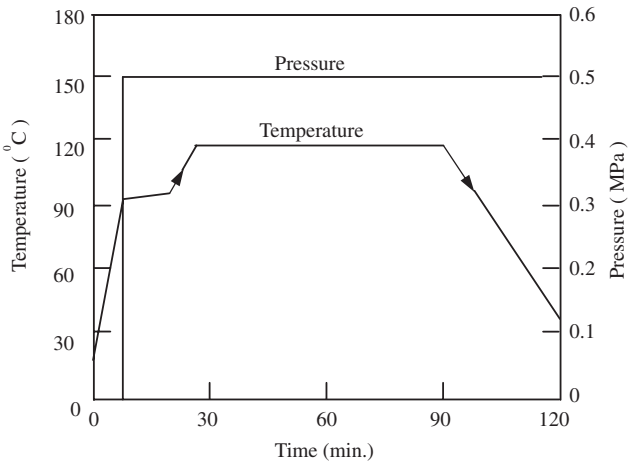

Fig. 6 Cure cycle for the manufacture of a composite plate

6. Demoulding and polishing the surface of the product to make it smooth.

5.2 First-ply failure testing

Some tests were performed to examine the first-ply failure loads of the composite plates. In these tests, the composite plates are simply supported upon the four steel channels of the fixture and subjected to the central transverse force until they fail. As shown in Fig. 7, the experimental apparatus for first-ply failure testing consisted of a load application system, a number of strain gauges, an AMS3 (Vallen, Germany) AE system with two AE sensors, a LVDT (linear variable differential transformer) displacement gauge, a data acquisition system, and a fixture for supporting the plate suspension system. A displacement gauge (LVDT) and a biaxial strain gauge were placed beneath the centre of the bottom surface of the plate for measuring the deformational parameters of the plate. The fixture was made of a grid pedestal and its associated parts, comprising galvanized steel channels, lift-out grid, and rigid grid mechanically fastened to the pedestal heads. These steel channels receive the plate, and the inside slots are to be joined with the edges of the base rib. During testing, with the load applicator acting at the centre of the panel, stroke control was adopted to determine the load–deflection relation for the specimens. The loading rate was slow enough for the inertia effect to be neglected. During testing, the stress waves produced in the specimen were recorded with the AE system using the two AE sensors attached to the specimen. The AE obtained were converted by the AMS3 (AE) system into a set of signal describers such as peak amplitude, energy, rise time, and duration, which were then used to identify the experimental first-ply failure load of the composite plate. For example, Fig. 8 shows the energy-applied load diagram for a $[30°/-30°/30°]_{-3S}$ composite plate produced by the AMS3 system. The first-ply failure load of the plate is determined by identifying the first major energy rise, as indicated in Fig. 8.

6 RESULTS AND DISCUSSION

6.1 Experimental verification

Before applying the aforementioned multi-level optimization procedure on the design of composite plates, it is worthwhile to demonstrate the accuracy of the present finite-element method in predicting the transverse deflection, the axial and lateral strains, and fibre angles of the composite plates. During testing, a displacement gauge (LVDT), biaxial strain gauge, and data acquisition system, were used to measure the deflection and strain data of the composite plates. A transverse central load of magnitude $P = 200$ N is

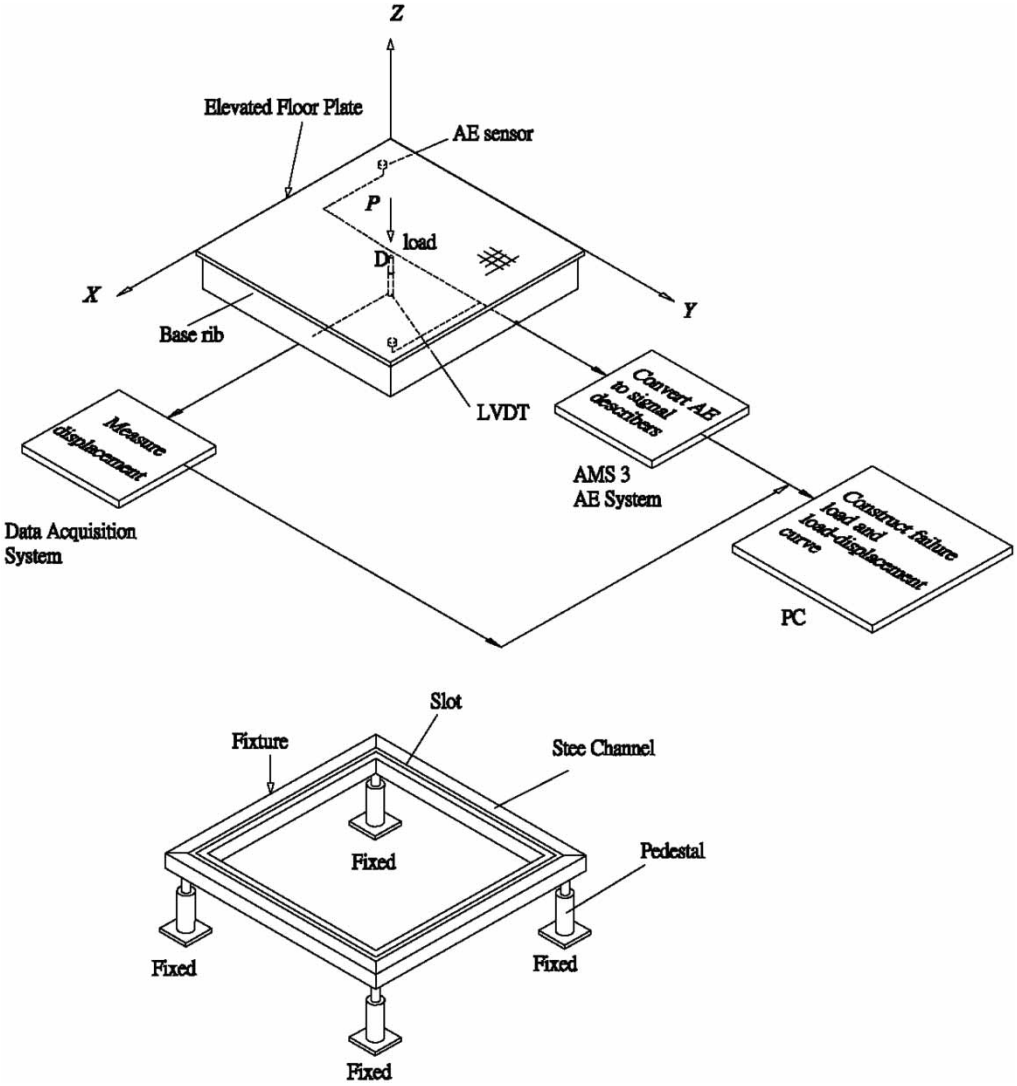

Fig. 7 Schematic description of the experimental set-up

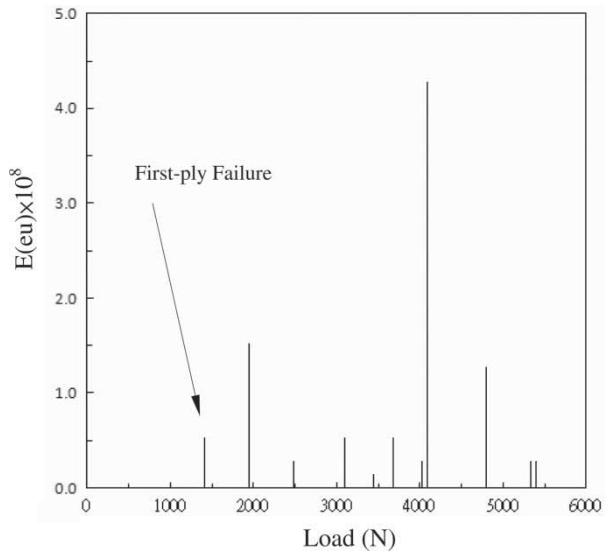

Fig. 8 Energy versus load produced by AMS3 AE system for a $[30°/-30°/30°]_{-3S}$ composite plate

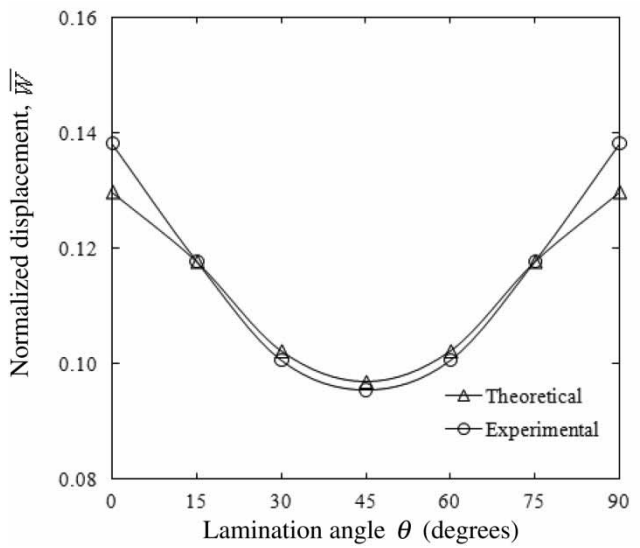

Fig. 9 Normalized centre displacement ($\bar{W} = W_c E_2 b h^3 / P_0 a^3$) versus lamination angle for anti-symmetric $[\theta/-\theta/\theta]_{-3S}$ plates

applied at the centre of the composite plate, with simply supported edges being plotted in Fig. 1. The actual dimensions of the plates used in the verification are length $a = b = 300$ mm, depth of the base rib $L = 35$ mm, number of layers NL = 18, and thickness $h = 4.68$ mm. The experimental and theoretical transverse deflections and strains obtained by the present method are given in Figs 9 and 10, respectively, for comparison. Tables 2 and 3 list the measured transverse deflections and strain pairs (axial and lateral strains), respectively, and compare with the theoretical results determined from four layer groups. It is noted that when compared with the experimental results, the solutions obtained from the theoretical analysis are fairly good solutions. In the above examples, the differences between the experimental and theoretical transverse deflections and strains of the composite plates are less than or equal to 3.67 per cent and 3.54 per cent, respectively.

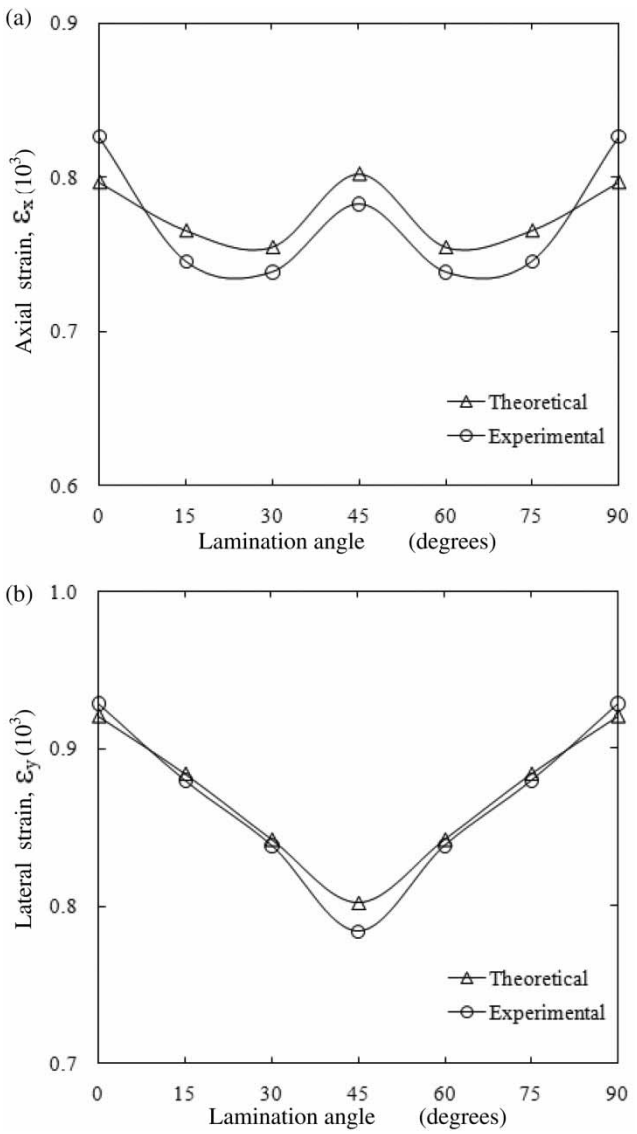

Fig. 10 Strain versus lamination angle for anti-symmetric $[\theta/-\theta/\theta]_{-3S}$ plates: (a) axial direction and (b) lateral direction

Table 2 Experimental and theoretical predictions of transverse deflections of a composite plate with various fibre layers $[\theta/-\theta/\theta]_{-3S}$ subjected to centre point load $P = 200$ N

Angle, θ (degree)	Theoretical transverse deflection, W (mm)	Experimental transverse deflection, $\bar{W}$ (mm)	Difference (%) $\lvert(W-\bar{W})/\bar{W}\rvert \times 100$
0	0.865	0.898	3.67
15	0.785	0.786	0.12
30	0.682	0.671	1.63
45	0.646	0.637	1.41

Table 3 Experimental and theoretical predictions of strain pairs of a composite plate with various fibre layers $[\theta/-\theta/\theta]_{-3S}$ subjected to centre point load $P = 200$ N

Angle, θ (degree)	Theoretical (I) ε_x ε_y	Experimental (II) $\bar{\varepsilon}_x$ $\bar{\varepsilon}_y$	Difference (%) $\lvert(\mathrm{I}-\mathrm{II})/\mathrm{II}\rvert \times 100$
0	796.83	826.14	3.54
	920.97	928.61	0.82
15	765.26	745.35	2.67
	884.37	879.76	0.52
30	754.36	738.42	2.15
	842.56	838.46	0.48
45	802.28	782.69	2.50
	802.28	783.84	2.35

6.2 Optimization

Some examples are given to illustrate the applications of the proposed multi-level optimization approach. The material properties and the dimensions of the simply supported plates used in the following optimum design are given in Table 1. The maximum stiffness of anti-symmetric $[\theta/-\theta/\theta]_{-3S}$ composite plates composed of 18 layers (equal ply thickness $h_i = 0.26$ mm) with various values for length a and aspect ratios were investigated. Figures 11 to 14 are the normalized displacement ($\bar{W}$) plots for the composite plate with aspect ratio $b/a = 1.0$ or 2.0 and length a varying from 46.8 to 468 mm subjected to transverse central load P. It is noted that the optimal fibre angles of the composite plate for $b/a = 2.0$ are 0° irrespective of the magnitude of length a, and the corresponding length-to-depth ratio varies from 4.1 to 30.2 (e.g. see Figs 13 and 14). In contrast, for $b/a = 1.0$, length a may have significant effects on the optimal fibre angle and the length-to-depth ratio (a/L). When length $a = 46.8$ mm, the optimal fibre angle θ and the corresponding length-to-depth ratio a/L are 15° and 4.3, respectively (Fig. 11); for length $a = 468$ mm, they are about 30° and

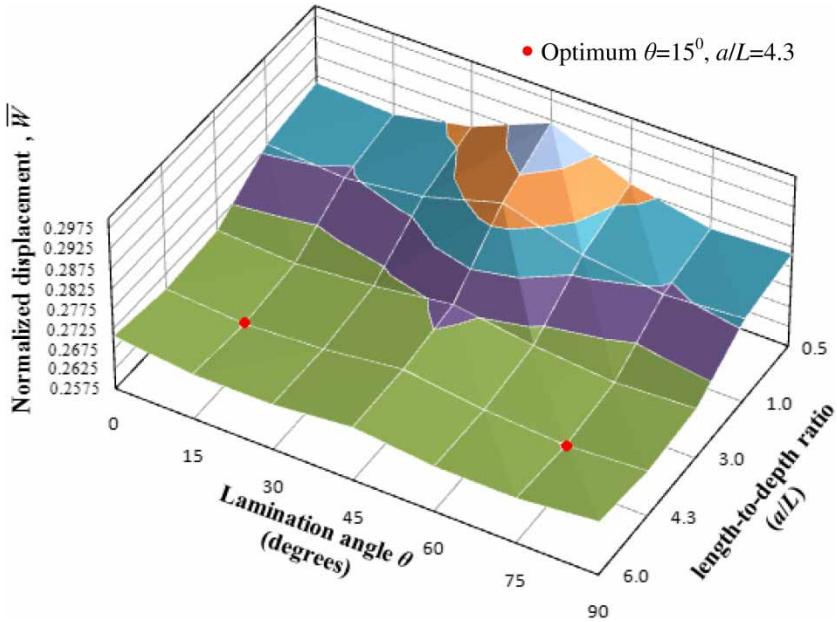

Fig. 11 Normalized centre displacement ($\bar{W} = W_c E_2 bh^3/Pa^3$) versus lamination angle and length-to-depth ratio for anti-symmetric $[\theta/-\theta/\theta]_{-3S}$ composite plates ($a = 46.8$ mm, $b/a = 1.0$)

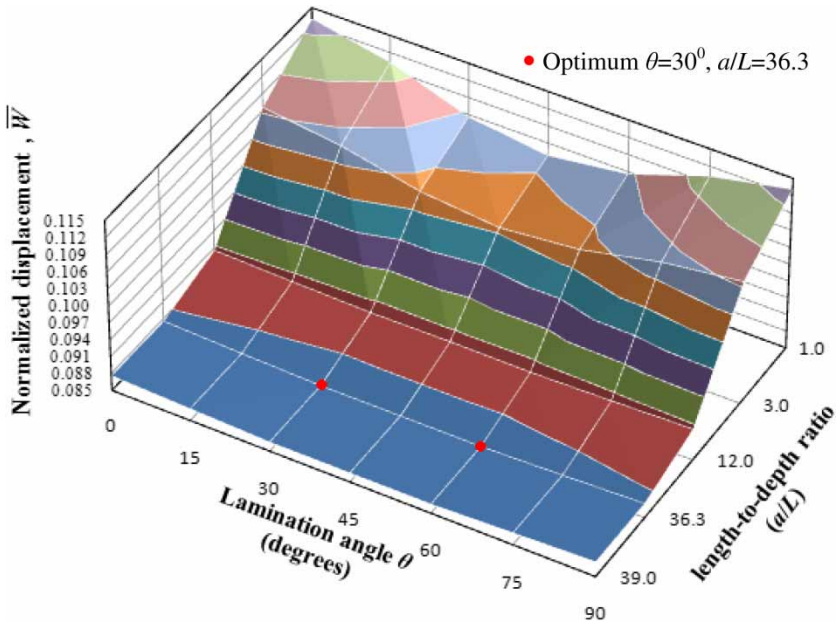

Fig. 12 Normalized centre displacement ($\bar{W} = W_c E_2 bh^3/Pa^3$) versus lamination angle and length-to-depth ratio for anti-symmetric $[\theta/-\theta/\theta]_{-3S}$ composite plates ($a = 468$ mm, $b/a = 1.0$)

36.3, respectively (Fig. 12). The approximate optimal fibre angles and the corresponding length-to-depth ratios for the global maximum stiffness of the composite plates with various lengths and aspect ratios extracted directly from Figs 11 to 14 are summarized in Table 4. The results show that length a and the aspect ratio have some effects on both the optimal fibre angles and the length-to-depth ratios of the composite plates. However, as length a increases, the effect on the optimal fibre angle becomes very small. It is also noted that for all the cases, the corresponding length-to-depth ratio has certain effects on the plate's

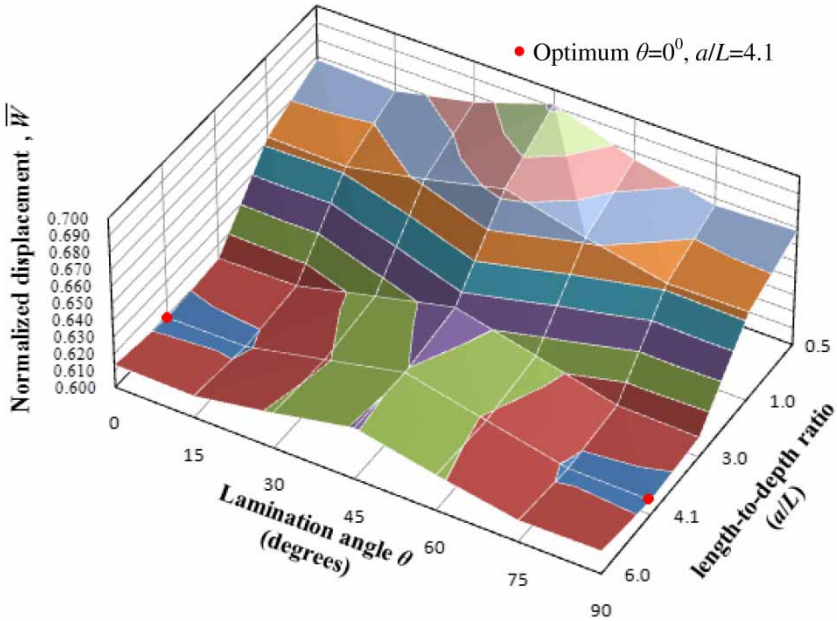

Fig. 13 Normalized centre displacement ($\bar{W} = W_c E_2 bh^3/Pa^3$) versus lamination angle and length-to-depth ratio for anti-symmetric $[\theta/-\theta/\theta]_{-3S}$ composite plates ($a = 46.8$ mm, $b/a = 2.0$)

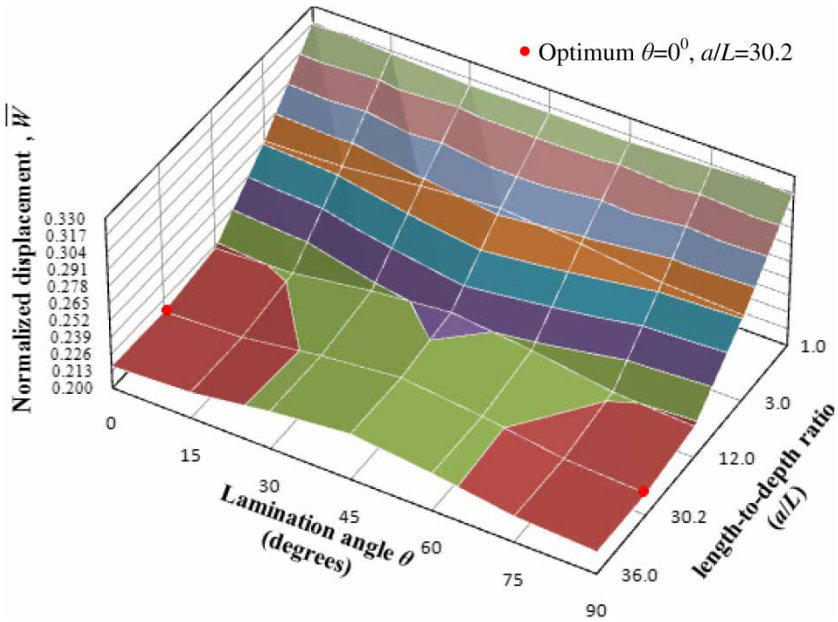

Fig. 14 Normalized centre displacement ($\bar{W} = W_c E_2 bh^3/Pa^3$) versus lamination angle and length-to-depth ratio for anti-symmetric $[\theta/-\theta/\theta]_{-3S}$ composite plates ($a = 468$ mm, $b/a = 2.0$)

maximum stiffness as the plate area increases. For example, in Table 4, as the plate area increases, the optimal depth of the base rib increases drastically when a increases from 46.8 to 936 mm, whereas the optimal depth of base rib changes only slightly for the aspect ratio changing from 1.0 to 2.0. In other words, the optimal depth of the base rib increases as the plate area increases. The results also reveal the fact that the optimal ply angles and the corresponding depth of the base rib have an important effect on the strength of the plate. On the basis of this design method, an elevated floor plate structure with lower stress in the base rib for a given central load can be designed.

Table 4 The optimal ply angles and the corresponding length-to-depth ratios of anti-symmetric $[\theta/-\theta/\theta]_{-3S}$ composite plates for maximum stiffness

	$h = 4.68$ mm															
	$a = 46.8$ mm				$a = 234$ mm				$a = 468$ mm				$a = 936$ mm			
b/a	θ (degree)	a/L	L (mm)	$\bar{W}$	θ (degree)	a/L	L (mm)	$\bar{W}$	θ (degree)	a/L	L (mm)	$\bar{W}$	θ (degree)	a/L	L (mm)	$\bar{W}$
1.0	15	4.3	10.9	0.267	30	20.9	11.2	0.094	30	36.3	12.9	0.086	30	59.4	15.7	0.083
1.5	15	4.3	10.9	0.405	0	16.7	14.0	0.172	0	30.4	15.4	0.159	0	52.7	17.8	0.153
2.0	0	4.1	11.4	0.608	0	16.7	14.0	0.235	0	30.2	15.5	0.216	0	49.7	18.8	0.208

$\bar{W}$: normalized centre displacement ($\bar{W} = W_c E_2 bh^3/Pa^3$).
L: depth of the base rib.

6.3 First-ply failure loads

According to the aforementioned optimization results, the optimal angle-ply orientations and the corresponding length-to-depth ratios of the composite plates for the maximum stiffness range from 0° to 30° and 4.1 to 59.4, respectively. In the present study, the experimental failure load results are treated as exact and the errors in theoretical results determined from three specimens for each lamination arrangement are indicated in Table 5. The dimensions of the laminated composite plates used in the first-ply failure analysis are length $a = b = 300$ mm, depth of the base rib $L = 35$ mm, number of layers NL = 18, and thickness $h = 4.68$ mm. In the theoretical failure analysis, failure is predicted to initiate at point D on the bottom surface of the central region of the plate, as shown in Fig. 7, and the theoretical failure locations have been confirmed by experimental observations. The present optimal angle-ply orientations of the laminated composite plate for the maximum stiffness are referenced to determine the angle-ply orientations of the laminated composite plate for experimental first-ply failure load ranging between 0° and 30°. The measured first-ply failure loads together with their average values and coefficients of variation (COVs) of the composite plates

Table 5 Theoretical and experimental predictions of first-ply failure loads for laminated composite plates with various fibre layers $[\theta/-\theta/\theta]_{-3S}$

		First-ply load F (N)						Ultimate failure load R (N)	Difference (%)		Failure location	
			Experimental (II)									
			Specimens									
Failure criterion	Angle θ (degree)	Theoretical (I)	1	2	3	Average (II)	COV (%)	Experimental (III)	(II − I)/ II × 100	(II/III) ×100	Point	Failure layer no.
Maximum stress (independent)	0	1330.0	1291	1238	1227	1252	2.73	5747	6.2	21.8	D	18
	10	1345.0	1375	1308	1298	1327	3.15	6920	1.4	19.2		18
	30	1391.0	1477	1404	1427	1436	2.60	7077	3.1	20.3		18
Maximum stress (polynomial)	0	880.3	1291	1238	1227	1252	2.73	5747	29.6	21.8	D	18
	10	919.0	1375	1308	1298	1327	3.15	6920	30.7	19.2		18
	30	965.0	1477	1404	1427	1436	2.60	7077	32.8	20.3		18
Maximum strain (independent)	0	1512.0	1291	1238	1227	1252	2.73	5747	20.7	21.8	D	18
	10	1518.0	1375	1308	1298	1327	3.15	6920	14.4	19.2		18
	30	1562.0	1477	1404	1427	1436	2.60	7077	8.8	20.3		18
Maximum strain (polynomial)	0	995.5	1291	1238	1227	1252	2.73	5747	20.5	21.8	D	18
	10	1039.0	1375	1308	1298	1327	3.15	6920	21.7	19.2		18
	30	1091.0	1477	1404	1427	1436	2.60	7077	24.0	20.3		18
Hoffman	0	845.5	1291	1238	1227	1252	2.73	5747	32.4	21.8	D	18
	10	883.0	1375	1308	1298	1327	3.15	6920	33.4	19.2		18
	30	927.0	1477	1404	1427	1436	2.60	7077	35.4	20.3		18
Tsai–Hill	0	1296.0	1291	1238	1227	1252	2.73	5747	3.5	21.8	D	18
	10	1350.5	1375	1308	1298	1327	3.15	6920	1.7	19.2		18
	30	1417.0	1477	1404	1427	1436	2.60	7077	1.3	20.3		18
Tsai–Wu	0	845.5	1291	1238	1227	1252	2.73	5747	32.4	21.8	D	18
	10	883.0	1375	1308	1298	1327	3.15	6920	33.4	19.2		18
	30	927.0	1477	1404	1427	1436	2.60	7077	35.4	20.3		18

are listed in Table 5. It is noted that the COVs of the measured first-ply failure loads are less than or equal to 3.15 per cent. It is also noted that when the arrangement of the fibre lay-ups is $[30^\circ/-30^\circ/30]_{-3S}$, the experimental first-ply failure load, $F = 1436$ N, and ultimate failure load, $R = 7077$ N, are much higher than those of the other arrangements. Regarding the capabilities of the adopted failure criteria in predicting first-ply failure load, it has been found that the maximum stress (independent), maximum strain (independent), and Tsai–Hill failure criteria can yield fairly good results with consistent accuracy for the composite plates. In particular, the Tsai–Hill failure criterion can predict first-ply failure load within a 1.5 per cent error. On the contrary, the analytical methods together with the Hoffman criterion show significant differences between the theoretical and experimental first-ply failure loads, which are greater than 35 per cent as shown in Table 5. The big difference between the first-ply and ultimate failure loads may have significant advantages for safety design of composite elevated floor plates. Hence, it is of obvious importance to extend the present experimental and theoretical analyses to first-ply failure load prediction of composite elevated floor plates. Therefore, the composite elevated floor plate will be safe enough if it is designed against the first-ply failure load.

7 CONCLUSION

In this article, a 3D laminated composite elevated floor plate was designed and manufactured by VARTM. To assess the feasibility of this material manufactured using the VARTM process, it is very important to understand the failure behaviour of these composite materials. The design of a laminated composite plate fabricated with fibre layers and the corresponding length-to-depth ratios and aspect ratios were presented. A comparison between the experimental approaches and the analytical methods was made to demonstrate the suitability of the failure criteria in predicting first-ply failure strength. The first-ply failure analysis of the composite plate was performed via the use of a suitable failure criterion. Results concerning first-ply failure and ultimate failure loads for the composite plates have been presented for comparison. Ultimate failure load is generally higher than first-ply failure load of a composite plate. It may be appropriate to use first-ply failure as a criterion for the design of laminated composite plates. A comparison between the theoretical and experimental results was carried out to validate the present method. Thus, the results presented in this article should be valuable for practical applications. In the present stage, however, no account is taken of interlaminar stresses such as the normal stress in three directions (through thickness direction). Accordingly, the present lamination theory is incapable of providing predictions of some of the stresses that actually cause delamination failure of a composite material. It is suggested that further research on failure analysis of laminates and development of appropriate failure criteria, based on principles of fracture mechanics, is needed.

ACKNOWLEDGEMENT

This research was supported by the National Science Council of the Republic of China under grant no. NSC 93–2212-E-157–003.

REFERENCES

1 **Albrecht, R. E., Gartnerv, R. W.,** and **Hazen, J. O.** *Floor panel for elevated floor assembly*. US Pat. 4 656 795, 1987.
2 **Hardwicke, C. S., Leffel, H. R.,** and **Spatoulas, G. S.** *Elevated floor plate*. US Pat. 4 745 715, 1988.
3 **Ray, G. F.** *Elevated floor panel and method of manufacturing same*. US Pat. 4 753 058, 1988.
4 **Hardwicke, C. S., Leffel, H. R.,** and **Spatoulas, G. S.** *Elevated floor plate*. US Pat. 4 825 603, 1988.
5 **Hardwicke, C. S., Leffel, H. R.,** and **Spatoulas, G. S.** *Elevated floor plate*. US Pat. Des. 306 350, 1990.
6 **Ikegami, K., Nose, Y., Yasunaga, T.,** and **Shiratori, E.** Failure criterion of angle ply laminates of fibre reinforced plastic and applications to optimize the strength. *Fibre Sci. Technol.*, 1982, **16**, 175–190.
7 **Soni, S. R.** A new look at commonly used failure theories in composite laminates. In Proceedings of the 24th AIAA/ASME/ASCE/AHS Structures, Structural Dynamics and Materials Conference, Lake Tahoe, Nevada, 2–4 May 1983, p. 171.
8 **Reddy, Y. S. N.** and **Reddy, J. N.** Linear and non-linear failure analysis of composite laminates with transverse shear. *J. Compos. Sci. Technol.*, 1992, **44**, 227–255.
9 **Reddy, J. N.** and **Pandey, A. K.** A first-ply failure analysis of composite laminates. *Comput. Struct.*, 1987, **25**, 371–393.
10 **Kam, T. Y.** and **Sher, H. F.** Nonlinear and first-ply failure analysis of laminated cross-ply plates. *J. Compos. Mater.*, 1995, **29**, 463–482.
11 **Kam, T. Y.** and **Jan, T. B.** First-ply failure analysis of laminated composite plates based on the layerwise linear displacement theory. *J. Compos. Struct.*, 1995, **32**, 583–591.
12 **Kam, T. Y., Chang, R. R., Sher, H. F.,** and **Chao, T. N.** Prediction of first-ply failure strengths of laminated composite plates using a finite element approach. *Int. J. Solids Struct.*, 1996, **33**, 375–398.
13 **Chang, R. R.** Experimental and theoretical analyses of first-ply failure of laminated composite pressure vessels. *J. Compos. Struct.*, 2000, **49**, 237–243.
14 **Chang, R. R.** and **Chu, J. M.** Predictions of first-ply failure of laminated composite shafts. *J. Expl Mech.*, 2003, **43**(2), 183–193.

15 *ANSYS release 8.0 documentation*, 2003 (ANSYS Inc, Canonsburg, PA, USA).

16 **Reddy, J. N.** A penalty plate-bending element for the analysis of laminated anisotropic composite plates. *Int. J. Numer. Meth. Engng*, 1980, **15**, 1187–1206.

17 **Tsai, S. W.** and **Hahn, H. T.** *Introduction to composite materials*, 1980 (Technomic Lancarter, PA).

18 **Reissner, E.** The effect of transverse shear deformation on the bending of elastic plates. *J. Appl. Mech., Trans. ASME*, 1945, **67**, 69–77.

19 **Kirsch, U.** *Optimum structural design*, 1981 (McGraw-Hill, New York).

20 **Young, W. B., Han, K., Fong, L. H.,** and **Liou M. J.** Flow simulation in molds with preplaced fibre mats. *Polym. Compos.*, 1991, **12**, 391–406.

21 **Young, W. B., Han, K., Fong, L. H.,** and **Liou, M. J.** Analysis of resin injection molding in molds with preplaced fibre mats, part I: permeability and compressibility measurements. *Polym. Compos.*, 1991, **12**, 30–38.

22 **Young, W. B., Han, K., Fong, L. H.,** and **Liou, M. J.** Analysis of resin injection molding in molds with preplaced fibre mats, part II: numerical simulation and experiments of mold filling. *Polym. Compos.*, 1991, **12**, 20–29.

23 **Sun, X. D., Li, S.,** and **Lee, L. J.** Mold filling analysis in vacuum-assisted resin transfer molding, part I: SCRIMP based on a high-permeable medium. *Polym. Compos.*, 1998, **19**, 807–817.

24 **Sun, X. D., Li, S.,** and **Lee, L. J.** Mold filling analysis in vacuum-assisted resin transfer molding, part II: SCRIMP based on grooves. *Polym. Compos.*, 1998, **19**, 818–827.

25 **Acheson, J. A., Simacek, P.,** and **Advani, S. G.** The implications of fibre compaction and saturation on fully coupled VARTM simulation. *Compos. Part A, Appl. Sci. Manuf.* 2004, **35**, 159–169.

APPENDIX

Notation

a, b	length
A_{ij}	components of laminate in-plane stiffness matrix
$\overline{A_{ij}}$	components of laminate thickness-shear stiffness matrix
B_{ij}	components of laminate bending in-plane coupling stiffness matrix
D_{ij}	components of laminate twist coupling stiffness matrix
h	total thickness of the laminate
h_i	thickness of ith layer
k_α, k_β	shear correction factors
L	depth of the base rib
M_i	moment result components
N_i	in-plane stress result components
NL	number of layers
P	transverse central load
Q_i	transverse shear stress result components
$Q_{ij}^{(m)}$	mth layer lamina stiffness coefficients
W	transverse deflection of the simply supported plate
W^0	reference value of W
Z_m	distance from mid-plane to the lower surface of the mth layer
θ	vector of the fibre layer directions
$\Phi(\boldsymbol{\theta}, L)$	multi-objective function